CHEMISTRY OF MATERIALS

Article

pubs.acs.org/cm

# Unique Reversible Crystal-to-Crystal Phase Transition—Structural and Functional Properties of Fused Ladder Thienoarenes

Yuichiro Abe,[†,‡,§] Victoria Savikhin,[#] Jun Yin,[⊥] Andrew C. Grimsdale,[†] Cesare Soci,[∥] Michael F. Toney,[#] and Yeng Ming Lam*[,†]

[†]School of Materials Science and Engineering, Nanyang Technological University, 50 Nanyang Avenue, Singapore 639798

[‡]Interdisciplinary Graduate School, Nanyang Technological University, Singapore

[§]Energy Research Institute at NTU (ERI@N), Nanyang Technological University, Singapore

[∥]School of Physical and Mathematical Sciences, Nanyang Technological University, Singapore

[⊥]KAUST Solar Center, Division of Physical Science and Engineering, King Abdullah University of Science and Technology, Thuwal 23955-6900, Saudi Arabia

[#]Stanford Synchrotron Radiation Lightsource, SLAC National Accelerator Laboratory, Menlo Park, California 94025, United States

Supporting Information

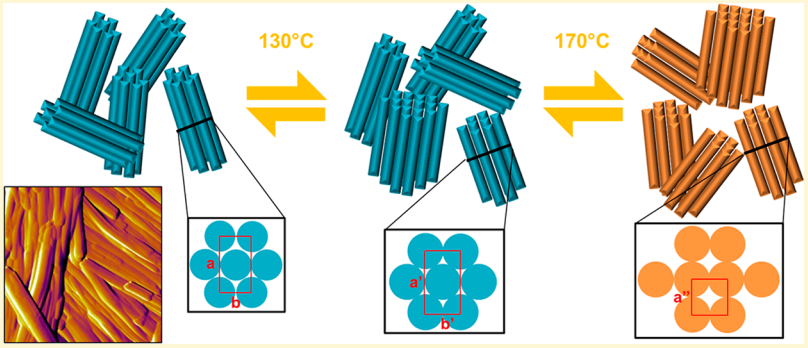


**ABSTRACT:** Donor−acceptor type molecules based on fused ladder thienoarenes, indacenodithiophene (IDT), and dithienocyclopenta−thienothiophene (DTCTT), coupled with benzothiadiazole, are prepared, and their solid-state structures are investigated. They display a rich variety of solid phases ranging from amorphous glass states to crystalline states, upon changes in the central aromatic core and side group structures. Most notably, the DTCTT-based derivatives showed reversible crystal-to-crystal phase transitions in heating and cooling cycles. Unlike what has been seen in $\pi$-conjugated molecules, variable temperature XRD revealed that structural change occurs continuously during the transition. A columnar self-assembled structure with slip-stacked $\pi-\pi$ interaction is proposed to be involved in the solid state. This research provides the evidence of unique structural behavior of the DTCTT-based molecules through the detailed structural analysis. This unique structural transition paves the way for these materials to have self-healing of crystal defects, leading to improved optoelectronic properties.

## INTRODUCTION

Establishing structure/property relationships in organic semiconductors is crucial for optimal design of molecules for applications in optoelectronic devices such as organic photovoltaics (OPV). Decades of intensive research into materials development have established some useful design strategies which contributed to the development of high performance solar cells in recent years. One such example is the $D_1-A-D_2-A-D_1$ type of small molecular donors used in small molecular organic photovoltaic (sm-OPV) devices.[1,2] This type of molecule has demonstrated impressive device results of up to 10% power conversion efficiency.[3−5] The active layer solid-state structures have also been investigated using both experimental and computational methods.[6−10] Controlling the solid-state structure and improving important properties such as charge transport properties could further improve the device performance.

In conjugated organic materials, charge transport properties depend very heavily on the packing structure of the molecules as the packing structure determines the $\pi$-orbital overlap. However, the packing structure is mainly stabilized by weak van der Waals interactions and often has several crystalline packing states (polymorphs) and loosely bonded mesophases (liquid crystalline states). Depending on their packing, these states have various degrees of $\pi$-orbital overlap and hence, different electronic properties. Thus, they provide an interesting

Received: March 26, 2017
Revised: August 13, 2017
Published: August 15, 2017





DOI: 10.1021/acs.chemmater.7b01226
Chem. Mater. 2017, 29, 7686−7696

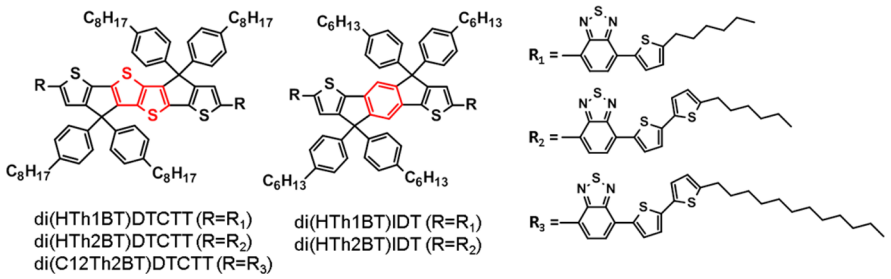


**Figure 1.** Chemical structures of DTCTT- and IDT-based small molecules.

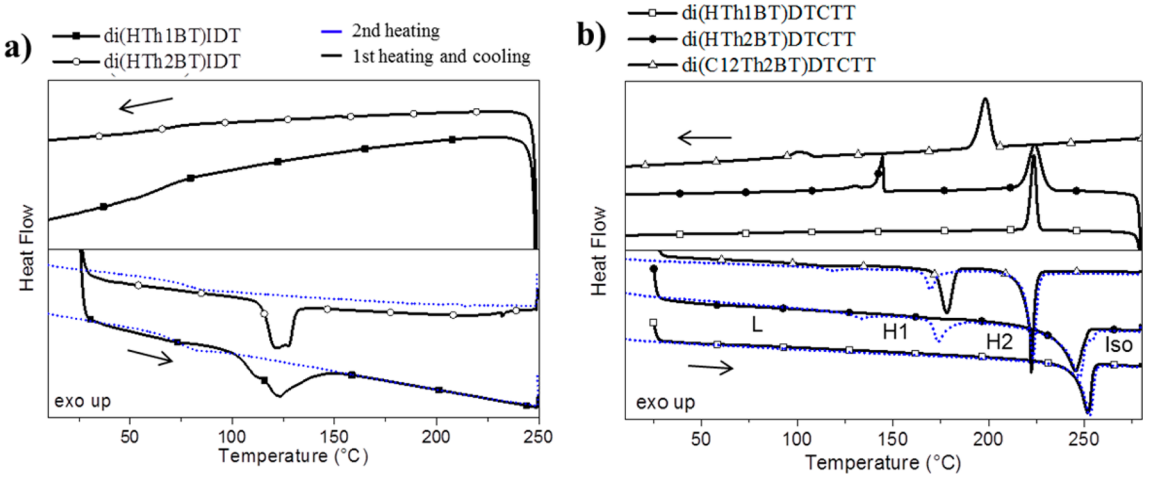


**Figure 2.** Differential scanning calorimetry (DSC) of IDT derivatives (a) and DTCTT derivatives (b); the black line is the first heating and cooling cycle, and the dotted blue line is the second heating cycle, scanned at 10 °C/min rate.

platform to investigate the intrinsic charge transport properties and the relationship between charge transport and packing structure.[11−13] Various attempts were made to access the ideal packing structures for charge transport properties. Certain polymorphic structures have been induced by applying external stimuli,[14,15] controlling crystallization environment,[16] and utilizing intermolecular interaction with additives.[17,18] Liquid crystalline semiconductors[19−23] have also recently emerged as candidates for sm-OPV due to the possibility of utilizing their uniquely ordered solid-state structures.

Previously, we have reported a dithienocyclopenta-thieno-[3,2-*b*]thiophene (DTCTT)-based molecular donor material for sm-OPV.[24] Comparative studies between the DTCTT and the structurally analogous indacenodithiophene (IDT)-based molecular donor, which has a benzene core instead of the thienothiophene in DTCTT, demonstrated enhanced crystallinity of the DTCTT-based molecule induced by the S−S interactions from the thienothiophene unit. In this study, a series of novel IDT- and DTCTT-based derivatives were synthesized (Figure 1) to elucidate their packing structure in the solid state and how this affects their optoelectronic properties. Special focus was placed on the molecular rearrangement dynamics in the reversible phase transition behavior seen in the DTCTT derivatives. This reversible phase transition, or enantiotropic phase transition, has been widely studied.[25,26] The structural reversibility and the associated properties of this transition are also interesting for optoelectronic,[27−31] ferroelectric,[32,33] and energy[34,35] applications. Moreover, the thermally induced structural reversibility was demonstrated to have a self-healing function, reported recently.[36] Structural investigation using X-ray diffraction techniques revealed that the DTCTT molecules organized in one-dimensional columns with slip-stacked self-assembly and showed phase transitions similar to columnar liquid crystals, while retaining their three-dimensional order. Our investigation of the relationship between their molecular structures and unique self-assembled structures, together with preliminary p-type transistor properties, will provide evidence of advanced crystal engineering of organic solids, which is a critical part for improving optoelectronic device performance.

## EXPERIMENTAL METHODS

**Sample Preparation.** The DTCTT- and IDT-based small molecules in Figure 1 were synthesized based on the synthetic scheme reported in our previous paper.[24] The synthetic and characterization details are available in the Supporting Information.

**Measurements.** Differential scanning calorimetry (DSC) was performed using DSC Q10 (TA Instruments) under nitrogen flow (scanning rate of 10 or 2 °C/min). The optical microscope image was recorded using Eclipse E600 microscope (Nikon), equipped with an Infinity-1 camera (Lumenera). The sample was placed on the hot plate Linkam THMS600, and heating rate and cooling rate were controlled by temperature controller Temmcon 102ST. A cross-polarization filter was applied in the case of taking the polarized optical image. No color filters or computational treatment was applied to the images. AFM images were obtained using Cypher S (Asylum Research) measured in tapping mode. Powder and thin-film X-ray diffraction patterns were measured using a D8 advanced (Bruker) with copper X-ray source. X-ray crystallographic analysis was performed using the 4-circles goniometer Kappa geometry AXS D8 Venture (Bruker), equipped with a Photon 100 CMOS active pixel sensor detector with a copper monochromatized X-ray radiation. Simultaneous SAXS and WAXS experiments were performed on a Nano-inXider (SW-L model) from Xenocs, Sassenage, France, using Cu K$\alpha$ radiation ($\lambda$ = 0.154189 nm).



DOI: 10.1021/acs.chemmater.7b01226
*Chem. Mater.* 2017, 29, 7686−7696

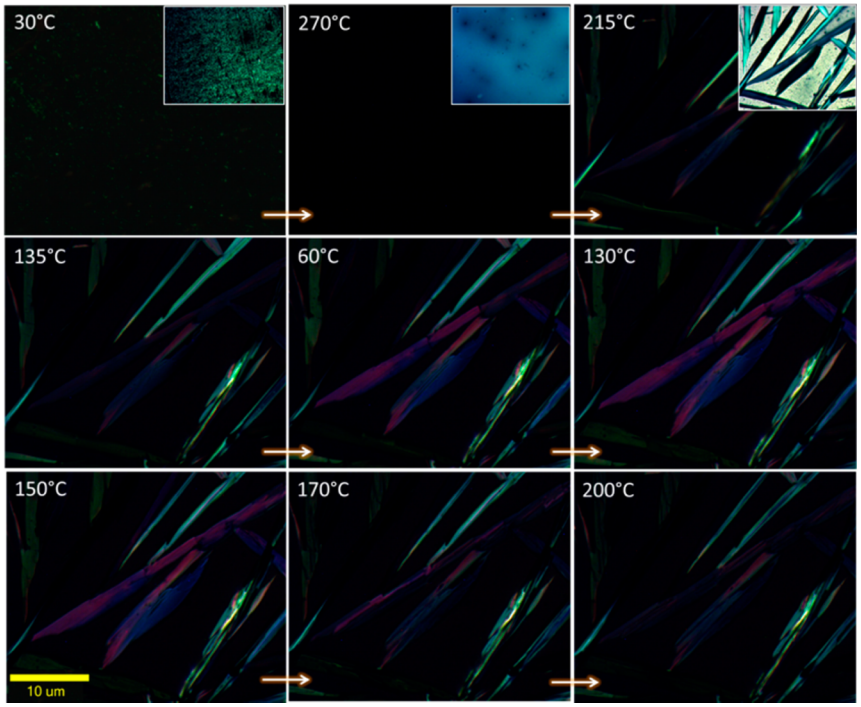


**Figure 3.** Polarized optical microscope image of di(HTh2BT)DTCTT at first heating, cooling, and second heating (thin film at 30 °C, isotropic liquid at 270 °C, cooling down to 60 °C, and second heating up to 200 °C). Inset is the image under bright light.

The sample was placed between two Kapton films of 50 $\mu$m, and in situ measurements were run as a function of temperature using the integrated temperature control stage Linkam HFX350. The thin-film sample for GI-WAXS was prepared by dissolving molecules in a mixed solution of chloroform:*o*-dichlorobenzene = 9:1 (5 mg/mL) and spin-coating the solution onto the substrates at 1000 rpm, resulting in an ca. 200 nm thin film. The measurement was done at Stanford Synchrotron Radiation Lightsource (SSRL) beamline 11-3 in grazing incidence mode with a 2D MARCCD detector at a sample−detector distance of 250 mm. Beam energy was 12.735 keV, and the incident angle used was 0.2°.

## RESULTS

**Molecular Design.** DTCTT- and IDT-based molecules with different side groups were synthesized to investigate the effect of the backbone and the side group structure on their self-assembly behavior. The side groups consist of benzo-[2,1,3]thiadiazole (BT) and alkyl thiophenes. The molecules with one thiophene (Th) unit in the side groups (R = $R_1$) were expected to have less structural freedom compared to those with two Th units (R = $R_2$). In addition, extended dodecyl alkyl groups (R = $R_3$) were introduced in place of the hexyl chains in DTCTT to investigate their effect on the reversible phase transition behavior. These IDT and DTCTT derivatives are interesting platforms to investigate the relationship between crystallinity and molecular structure as any slight change in chemical structures can result in the formation of different phases ranging from amorphous phase to crystalline phases with several crystalline polymorphs. Their phase transition behavior will be discussed in the following sections.

**Reversible Phase Transition Behavior.** The difference in the backbone structure of both the IDT and DTCTT compounds is found to have a distinct impact on the thermal behavior. The differential scanning calorimetry (DSC) graphs are shown in Figure 2, and the thermodynamic properties are summarized in Table S2. In Figure 2a, both the IDT derivatives showed glass transition temperatures of around 70 °C on cooling after their initial melting at around 110 °C. On the second cycle, melting and recrystallization are not observed, indicating they form a glass-supercooled liquid phase.[37] On the other hand, the DTCTT derivatives have crystalline nature as recrystallization peaks can be observed after their initial melting (melting at 245, 235, and 221 °C and crystallization at 226, 230, and 203 °C for R = $R_1$, $R_2$, and $R_3$ derivatives, respectively). In addition, cooling at 10 °C/min speed after the melting causes additional peaks for R = $R_2$ and $R_3$ derivatives. These transition peaks appeared reversibly even on the third and fourth heating-and-cooling cycle (Figure S2). Initially, this behavior was thought to be a thermotropic liquid crystalline phase transition, but the observation under polarized optical microscope (POM, Figure 3 for R = $R_2$ and Figure S3 for R = $R_3$) indicates this is a reversible crystal-to-crystal phase transition. From low to high temperature, each phase is assigned as L, H1, and H2 before melting into an isotropic liquid. These structure assignments are based on X-ray diffraction results presented in detail in the following discussion.

Under cross-polarization filters, a di(HTh2BT)DTCTT (R = $R_2$) film was placed on a hot plate (Figure 3 at 30 °C) and heated to 270 °C, which is above its melting temperature. No polarized light was observed at this temperature, indicating an isotropic liquid state. Upon cooling, crystallization took place, forming leaf-like crystals, and on further cooling, a subtle color change was observed at around 130 °C under the cross polarizers, indicating a phase transition and reorganization of the molecules. On the second heating cycle, similar phase transition behavior was observed at 130 °C, and further heating up to 170 °C resulted in cracks in the crystals. This observation matches well with the phase transition peaks observed in the DSC graphs (mixture of H2/H1/L transition at 145−125 °C on cooling, L/H1 transition at 128 °C and H1/H2 transition at


DOI: 10.1021/acs.chemmater.7b01226
*Chem. Mater.* 2017, 29, 7686−7696

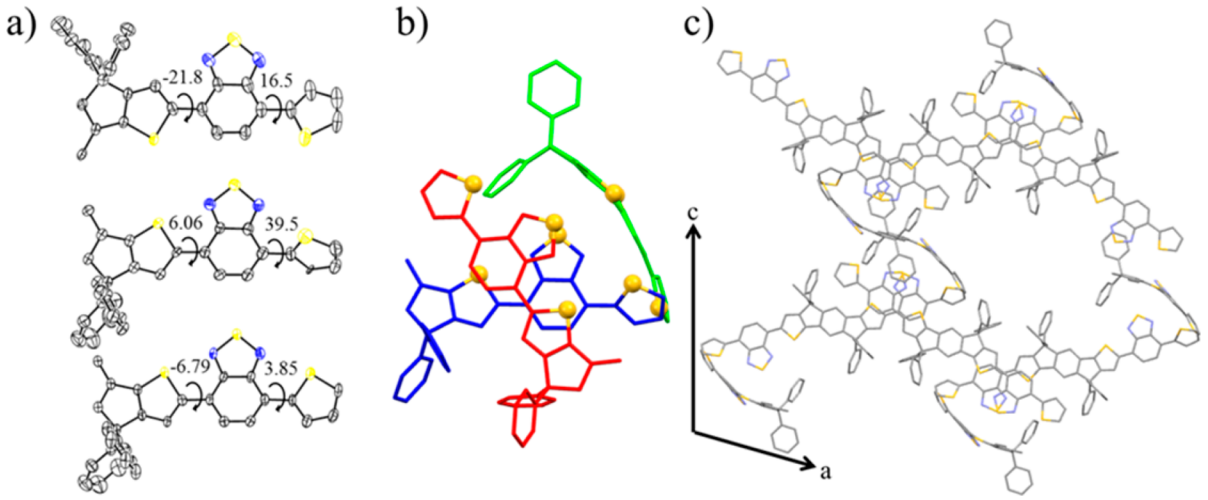


**Figure 4.** Model structures solved using single crystal X-ray diffraction of di(HTh1BT)IDT: (a) ORTEP image of crystallographically independent molecular units with ellipsoids drawn at 50% probability, (b) trimer structure with sulfur atoms in ball-and-stick model, and (c) molecular packing structure perpendicular to *b*-axis. C, N, and S atoms are shown as black, blue, and yellow, respectively. Alkyl chains and protons are omitted for clarity.

170 °C on second heating). It is worthwhile to note that a slower cooling rate did not change the shape of the DSC curve, but a faster cooling rate (higher than 30 °C/min) induced a "frozen" phase which did not show structural reversibility when observed under the POM and XRD (Figure S4).

The di(C12Th2BT)DTCTT (R = $R_3$) also exhibits three phases as can be seen in the DSC graph (mixture of H2/H1/L transition at 108−100 °C on cooling, L/H1 transition at 113 °C, and H1/H2 transition at 166 °C on heating), but no obvious morphological change was observed in the POM images. This implies that the structural reorganization takes place in a different manner from that of di(HTh2BT)DTCTT. It also showed scan rate-dependent DSC behavior; a slower scanning rate (such as 2 °C/min) makes the crystal-to-crystal phase transition peaks sharper, and peak splitting of the H2/H1/L transition on cooling and the H1/H2 transition on heating were observed (Figure S5). This implies existence of additional polymorphic states at these temperatures. These phase assignments are corroborated by evidence presented in the following discussion.

**Structural Analysis of IDT Derivatives.** We will first focus on the structural analysis of IDT derivatives as these are good reference materials for the analysis of the solid-state behavior of the DTCTT derivatives. Although both IDT derivatives showed amorphous nature (glass-supercooled liquid phase) in the thermal studies, they can be crystallized from a suitable mixed solvent system such as acetone/chloroform; their powder XRD data (Figure S6) represent a typical peak pattern for crystalline samples. On the other hand, thin film XRD data had no peaks and post-treatment, such as thermal/solvent vapor annealing did not change these amorphous patterns. The difficulty for the IDT derivatives to form ordered structures in the thin film originates from its molecular structure. The presence of four hexylphenyl groups on the sp3 carbon of the IDT moiety hinders strong $\pi-\pi$ stacking. A poor solvent, such as acetone, is thus necessary to induce nucleation through solvent−solute interactions[38] and/or solvophobic effects.[39,40]

A single crystal of di(HTh1BT)IDT (R = $R_1$) was grown, and its self-assembled structure was studied using single crystal XRD (Figure 4). Since the molecule has an inversion center on the central benzene ring, half of the molecular structure was solved as an asymmetric unit. The crystal is monoclinic with space group *C*2/*c* ($a$ = 23.73, $b$ = 27.78, $c$ = 38.16 Å; $\beta$ = 100.1°; $Z$ = 8). Three structural isomers are obtained, which have different rotation angles between the IDT, BT, and Th units (Figure 4a). Coughlin and co-workers studied the rotational free energy of similar compounds and discussed its relationship with the structural factors.[6,7] Multiple nonbonding interactions such as $\pi-\pi$ interactions, steric hindrance, and electrostatic forces compete with each other, and when these interactions work together to stabilize the rotation angle, a "conformational lock" occurs. Three rotational isomers are formed in the di(HTh1BT)IDT crystal, implying that the intermolecular interactions are so weak that they allow more than one stable rotational isomer. The trimer structure shown in Figure 4b indicates the lack of $\pi-\pi$ stacking despite the elongated conjugation length. In fact, one of the rotational isomers has a high dihedral angle of 38.3°, and the entire molecule is distorted along the long axis (Figure 4c). The calculated close atomic distances suggest that the S−S interactions among BT−BT, BT−IDT, and Th−Th play a key role in stabilizing the trimer structure instead of the $\pi-\pi$ or CH−$\pi$ interactions. Incorporation of heteroatoms larger than carbon facilitates the overlap of $\pi$-orbitals; the S−S interaction is especially well-known to enhance the hole mobility through this effect.[41−43]

**Structural Analysis of DTCTT Derivatives in Crystal.** The DTCTT derivatives were also recrystallized from the acetone/chloroform solvent system. Although single crystals of suitable size for single crystal XRD were not obtained, other X-ray diffraction techniques were used for structural analysis of the DTCTT derivatives. Powder XRD patterns were collected from the DTCTT samples prepared by grinding crystals (Figure 5). Major peaks of di(HTh1BT)DTCTT (R = $R_1$) are seen at $2\theta$ = 4.97, 8.29, 9.82, and 20.0° which correspond to *d*-spacing of 17.8, 10.7, 9.0, and 4.44 Å. As for di(HTh2BT)-DTCTT (R = $R_2$), weak peaks at small angle regimes indicate the lack of clear long-range order. However, subsequent annealing at 200 °C induced structural reorganization, resulting in a different peak pattern at $2\theta$ = 4.25, 5.00, and 5.68° which corresponds to *d*-spacing of 20.8, 17.7, and 15.6 Å. These


DOI: 10.1021/acs.chemmater.7b01226
*Chem. Mater.* 2017, 29, 7686−7696

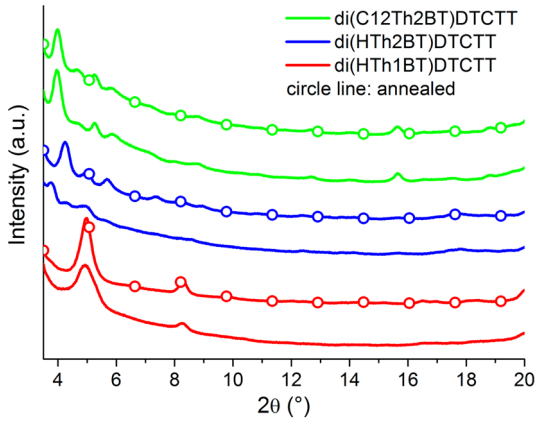


**Figure 5.** Powder XRD patterns of DTCTT derivatives. Recrystallized samples were ground and used as powder samples. The same annealing condition of 200 °C for 3 min was applied for all samples.

results indicate that the packing structure of di(HTh2BT)-DTCTT is sensitive to heating and mechanical deformation (grinding), and this sensitivity seems to be a factor in inducing the reversible phase transition that occurs in the crystal. The di(C12Th2BT)DTCTT (R = $R_3$) have strong peaks in both the small and wide angle regimes. The origin of peaks in the wide angle regime is not clear, but the distance is close to the van der Waals radius of the sulfur atoms, and thus they may be due to the aromatic groups incorporated with sulfur atoms which have electron rich planes and result in strong diffraction. The longer alkyl chains and two thiophene rings seem to assist in stabilizing the ordered structure.

The temperature-variable small and wide-angle X-ray scattering (SWAXS) was performed to investigate the reversible phase transition behavior of di(HTh2BT)DTCTT (R = $R_2$). The sample was first melted at 270 °C on a hot plate and then cooled at a rate of 10 °C/min, the same conditions as in the DSC measurements presented earlier. The diffracted X-rays were recorded using a 2D detector, and the diffractogram was generated by integrating their intensities with respect to the scattering vector. The diffraction was recorded at varying temperatures (from 25 to 230 °C and back to 25 °C) at a 5 °C step. As shown in the color map (Figure 6), the three phases are clearly observed (L, H1, H2, and back to H1, L phases), corresponding well with the transitions seen in the DSC studies. For clarity, the diffraction patterns of only the heating up cycle, from 25 to 230 °C, are plotted in Figure 7. At 25 °C, which corresponds to the L phase, two peaks ($q$ = 0.340 and 0.342 Å$^{-1}$) appear at low $q$ (Figure 7a). Upon heating, these peaks shift in a different manner; the peak that was originally at 0.342 Å$^{-1}$ shifts to lower $q$ while the peak at 0.340 Å$^{-1}$ shows little shift. This peak position behavior suggests anisotropic thermal expansion of the lattice parameters often seen in organic crystals.[44−46] Around 130 °C, the peaks at low $q$ exhibit a continuous structural change but shift very sharply at 135 °C, and both peaks separate out further ($q$ = 0.324 and 0.345 Å$^{-1}$) at 150 °C in the H1 phase. Above 175 °C, a drastic structural change takes place and new peaks appear ($q$ = 0.273 and 0.389 Å$^{-1}$), corresponding to the phase transition from H1 to H2. In this way, the different phases can be identified by XRD peak positions. However, since the phase transition from L to H1 occurs more gradually with ramping temperature, we have attempted to separate peak shift associated with phase transition from thermal expansion. The linear expansion of the two major peaks is plotted over the temperature range (Figure S7). A slope of the relative change in $d$-spacing vs temperature line is proportional to the thermal expansion coefficient. The coefficients of the two peaks originally at 0.340 and 0.342 Å$^{-1}$ are calculated to 5.3 × 10$^{-5}$ and 2.1 × 10$^{-4}$ K$^{-1}$ in the temperature range of the L phase (25−95 °C); the similar value was reported in organic crystals.[46−48] At a high temperature range around 130 °C, steps of slope are seen and very large negative and positive discontinuities are observed which identify the phase transition from L to H1. Peaks in the wide angle regime ($q$ = 1.25−1.5 Å$^{-1}$) (Figure 7b), which will correspond to $d$ = 4.19−5.03 Å, also changed their patterns, indicating a change in the packing mode. The fact that the high $q$ peaks are weak, together with the fact that the L to H1 phase transition appears to take place gradually, suggests that this structural reorganization has a very strong similarity to that of the liquid crystalline materials. Attempts to assign each phase were made and are discussed in a later section.

The same temperature-variable XRD measurement was performed for di(C12Th2BT)DTCTT (R = $R_3$). The sample was first melted at 250 °C and then cooled at a rate of 10 °C/min. The X-ray diffraction patterns were recorded during

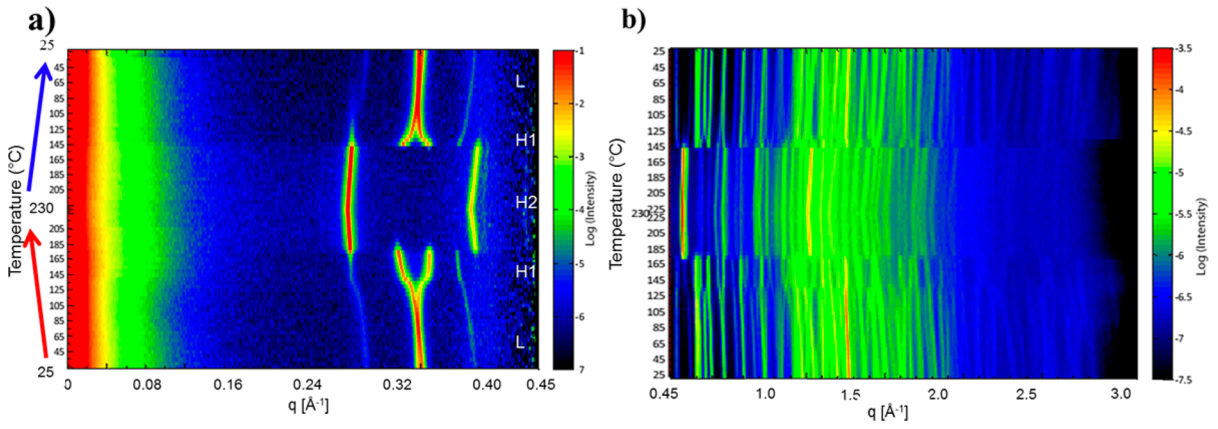


**Figure 6.** X-ray scattering image of di(HTh2BT)DTCTT in the (a) small angle regime and (b) wide angle regime in the color map at different temperatures. Scattering patterns were recorded by changing temperatures in a cycle of heating from 25 to 230 °C (before the melting temperature) and cooling at 230 to 25 °C with a 5 °C step. The sample was prepared by melting before slow cooling at a rate of 10 °C/min. The intensity is depicted with color bar in logarithmic scale on each regime. Note the small discontinuity in the peak positions at the L to H1 transition.



DOI: 10.1021/acs.chemmater.7b01226
Chem. Mater. 2017, 29, 7686−7696

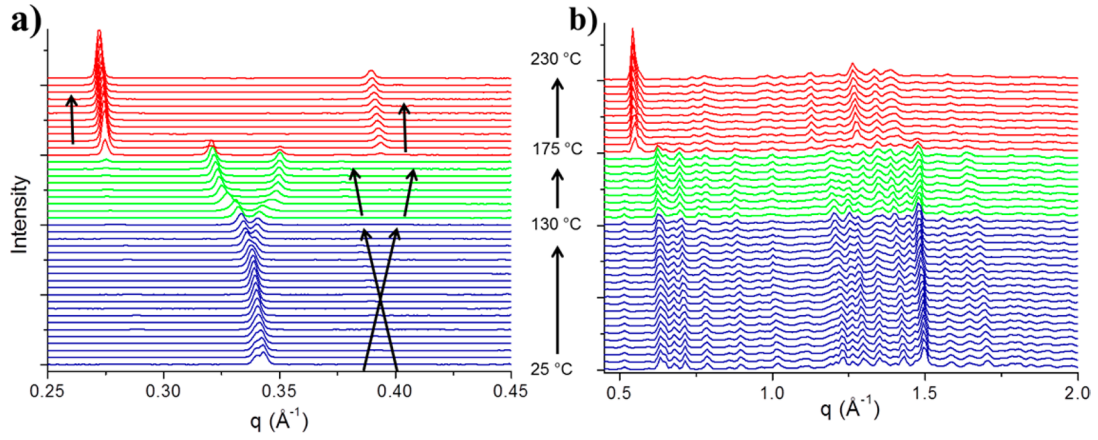


**Figure 7.** X-ray scattering patterns of di(HTh2BT)DTCTT in the (a) small angle regime and (b) wide angle regime when heating from 25 to 230 °C with a 5 °C step (blue, green, and red color correspond to L, H1, and H2 phases, respectively).

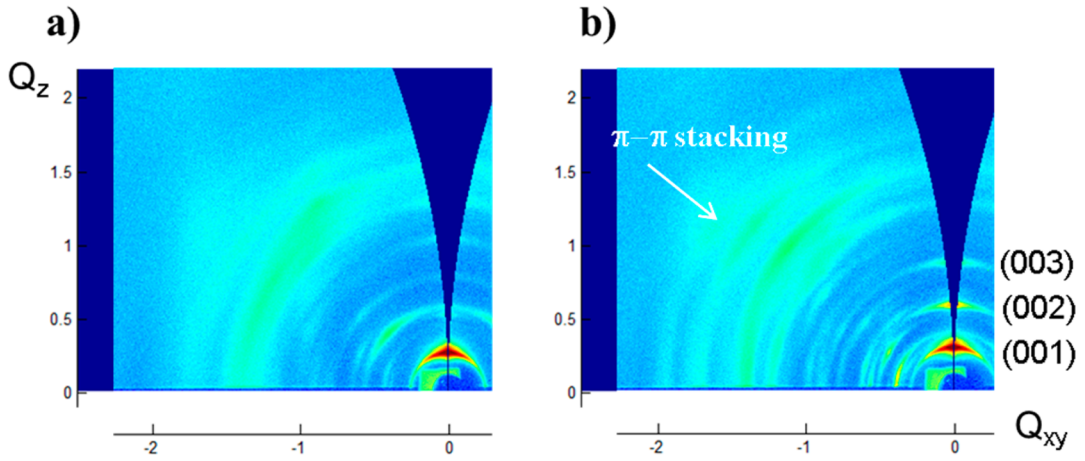


**Figure 8.** 2D GI-WAXS diffraction patterns of di(HTh2BT)DTCTT of (a) as spun film and (b) annealed film. Spin-coated film on silicon substrate was thermally annealed at 200 °C for 5 min.

heating and cooling cycle (25 to 200 °C and then back to 25 °C again) (refer to Figure S8 for the color map and Figure S9 for the diffraction patterns). Three major peaks ($q$ = 0.25, 0.33, and 0.41 Å$^{-1}$) appear in the small angle regime at 30 °C, which gradually shifts to lower angle upon heating. At 125 °C, the phase transition from L to H1 takes place, and the peak at 0.41 Å$^{-1}$ shows discontinuity (with peaks at $q$ = 0.24, 0.32, and 0.39 Å$^{-1}$ at 150 °C). Upon further heating, the phase transition of H1/H2 takes place and the middle peak disappears ($q$ = 0.24 and 0.39 Å$^{-1}$ at 200 °C). This diffraction pattern of the H2 phase resembles that of di(HTh2BT)DTCTT at the high temperature. At this temperature, alkyl chains gain sufficient freedom to move, and, thus, intermolecular interactions between the backbone structures become dominant for stabilizing the structure. Less contribution from the alkyl chains is assumed to result in the similar packing structure. Upon cooling, however, the middle peak intensity remains weak and distinct reversibility was not observed. In this measurement, cooling rate of 10 °C/min was applied to the sample but di(C12Th2BT)DTCTT showed scan-rate dependence in the DSC measurement. It seems the packing structure of di(C12Th2BT)DTCTT reorganizes more slowly compared to that of the di(HTh2BT)DTCTT. Due to the complexity of this kinetic factor, we mainly focused on the structural assignment of di(HTh2BT)DTCTT in the following discussion.

**GI-WAXS of di(HTh2BT)DTCTT in Thin Film.** Grazing-incidence small- and wide-angle X-ray scattering (GI-WAXS) was performed on the thin film sample of di(HTh2BT)-DTCTT using the synchrotron X-ray source. The thin film was prepared by spin coating from solution on silicon substrates (as-spun sample) and subjected to thermal annealing at 200 °C for 5 min (annealed sample). Structural reorganization was detected upon the thermal annealing, but the film structure did not return to the original phase, unlike its crystalline phases. The as-spun film (Figure 8a) showed a strong diffraction peak at $d$ = 23.9 Å along Qz, or the out-of-plane direction. Diffraction peaks at higher Q, corresponding to distances of 3.5−5 Å, which are typical $\pi-\pi$ stacking distances for aromatic molecules, are observed off axis (have nonzero Qxy and Qz components). These results suggest that the molecules adopt an edge-on mode of packing structure: the out-of-plane peak corresponds to periodicity along the alkyl stack direction, and the off-axis higher Q peaks correspond to packing along the $\pi-\pi$ stacking direction in slip-stacked manner (see below for more discussion on the slip stacking). This general observation is true for both as-spun and annealed films. In the annealed film (Figure 8b), molecular reorganization takes place, and the two scattering patterns have distinct peak positions and intensities.



DOI: 10.1021/acs.chemmater.7b01226
Chem. Mater. 2017, 29, 7686−7696

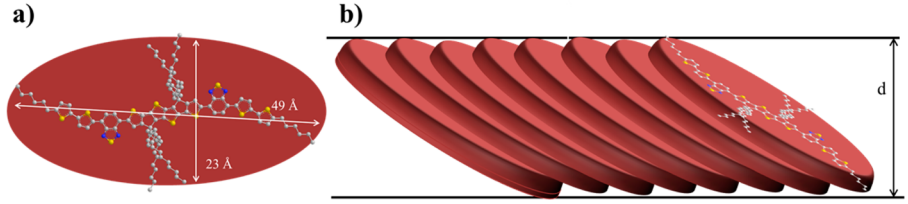


**Figure 9.** Schematic illustration of the molecular self-assembly: (a) optimized geometry of di(HTh2BT)DTCTT and (b) plausible 1D organized molecular self-assembly of di(HTh2BT)DTCTT with a projected diameter of *d*.

The strong peak along the out-of-plane direction ($d$ = 23.9 Å in as-spun film) shifts to $d$ = 21.4 Å with multiple reflections along the Qz direction, indicating the lamellar structure of (001), (002), and (003) reflections. Broad off-axis peaks ($d$ = 3.5−5 Å in as-spun film) become more intense with a certain degree of smearing. The annealed sample gives insight into the thermodynamically stable form of the molecule. Thermal energy allows molecules to reorient into an ordered packing structure, having both a long-range lamellar structure and a more ordered slip-stacked mode of $\pi-\pi$ stacking.

**Self-Assembled Structure of di(HTh2BT)DTCTT in the Reversible Phase Transition States.** Based on the above structural analysis, we attempted to assign the self-assembled structure of di(HTh2BT)DTCTT to its reversible phase transition states. The single molecular geometry was optimized using the DFT method with a hybrid function of B3LYP/6-31G(d,p). As shown in Figure 9a, the molecule has dimensions of 49 Å along the main axis of conjugation and 23 Å along the axis of the octyl phenyl groups. As revealed by X-ray crystallography, the structure of di(HTh1BT)IDT shows flexibility in the angles between the aromatic groups. Di-(HTh2BT)DTCTT is also assumed to form such rotational isomers, and the structure can be represented as an ellipsoid plane (Figure 9a). Based on GI-WAXS measurement of the di(HTh2BT)DTCTT, we speculate a model of the molecular self-assembly as illustrated in Figure 9b, having a one-dimensionally organized structure with slip-stacked manner of assembly so as to form a lamellar structure with a *d*-spacing of 21.4 Å. The samples prepared by the chloroform/acetone recrystallization process were found to crystallize in a fiber-like morphology, as revealed by atomic force microscopy (AFM) (Figure S10a,b). Those crystals can grow over 1 $\mu$m in length with a diameter ranging between 50 and 200 nm. Crystals of $\pi$-conjugated molecules tend to grow along the $\pi$-stacking direction.[49] The crystal growth of di(HTh2BT)DTCTT is also assumed to be driven by the slip-stacked $\pi-\pi$ stacking, which is speculated to form similar 1D organized structures in the crystal.

In order to validate our assumption in Figure 9b, the dimer structure determined from the geometry of the 1D organized molecular self-assembly was modeled using DFT calculation with the dispersion-corrected WB97XD function as a basis set. This function was selected for the calculation because it takes account of the effect of neighboring segments and so is suitable for modeling aromatic backbones.[50] The initial coordination (Figure S11) was taken from the geometry of the 1D organized structures in Figure 9b with the diameter $d$ = 23.0 Å. The diameter was extracted from the diffraction peak in the H2 phase. At high temperatures, alkyl chains show high flexibility, and this structure is believed to be a more suitable initial coordination for the molecular simulation. A stable dimer structure was successfully obtained from the modeling, as shown in Figure 10. In the stabilized structure, the distance between the two molecules is small near the center of the

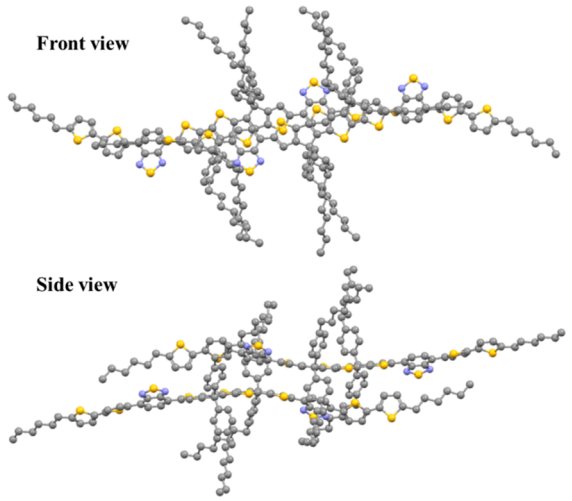


**Figure 10.** Slip-stacked dimer structure of di(HTh2BT)DTCTT. The structure was optimized using DFT calculation with WB97XD/6-31(d,p) as a basis set.

dimer. The distortion of the aromatic backbone is observed, and this is especially pronounced in the peripheral thiophene groups. The combination of the strong interaction between the central cores and the high flexibility of the end parts of the side groups could be the reason for sensitivity of the packing structure to temperature and grinding. The fact that the di(HTh1BT)DTCTT (R = $R_1$), unlike the other the DTCTT-based derivatives (R = $R_2$ and $R_3$), did not show a reversibility in the solid state indicates that an additional thiophene ring plays a key role in imparting structural flexibility, beneficial for the molecular reorganization.

Finally, the packing structures of the three phases (L, H1, and H2 phases) were analyzed using structural data obtained in the temperature variable SWAXS measurement shown in Figure 11. The gradual phase transition behavior from the L to the H1 phase resembles the typical behavior observed for columnar liquid crystals.[20,23,51−53] In such systems, a hexagonal (100) peak gradually splits into tetragonal (110) and (200) peaks according to the temperature. Structural assignment of columnar liquid crystalline materials has been studied for a long time[54] and applying the 2D lattice symmetricity into this system partially explained the phase transitions observed. The postulated packing structures of each phase are illustrated in Figure 12. The L phase at 30 °C is assigned as "pseudo-hexagonal" centered-rectangular phase ($C2mm$) with the lattice parameters $a$ = 36.6 Å and $b$ = 21.5 Å.[55] Upon heating, the shrinkage of the $a$-axis and the expansion of the $b$-axis gradually transforms the material into the H1 phase with $a$ = 36.0 Å and


DOI: 10.1021/acs.chemmater.7b01226
Chem. Mater. 2017, 29, 7686−7696

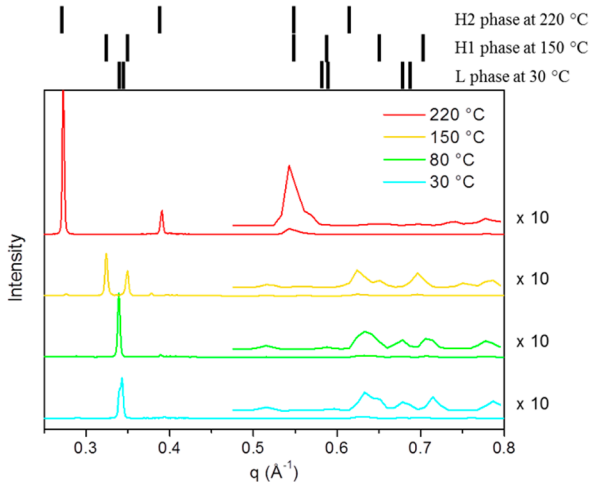


| Phase | $d_{obs}$/ Å | $d_{calcd}$/ Å | Millar indices |
|---|---|---|---|
| L at 30 °C | 18.5 | 18.5 | (11) |
| *C2mm* | 18.4 | 18.3 | (20) |
| a= 36.6 Å | 12.2 | 10.8 | (02) |
| b= 21.5 Å | 9.54 | 10.6 | (31) |
| | 9.27 | 9.27 | (22) |
| | 8.8 | 9.15 | (40) |
| H1 at 150 °C | 19.4 | 19.4 | (11) |
| *C2mm* | 18.2 | 18 | (20) |
| a= 36.0 Å | 12.2 | 11.5 | (02) |
| b= 23.0 Å | 10.1 | 10.6 | (31) |
| | 9.65 | 9.69 | (22) |
| | 9.03 | 9 | (40) |
| H2 at 220 °C | 23 | 23 | (11) |
| *P4mm* | 16.1 | 16.3 | (20) |
| a= 23.0 Å | 11.6 | 11.5 | (02) |
| | 11 | 10.3 | (31) |

**Figure 11.** Intensity vs 2$\theta$ plot of SWAXS data of di(HTh2BT)DTCTT at different temperatures. The calculated peak positions with each space group are shown as black lines.

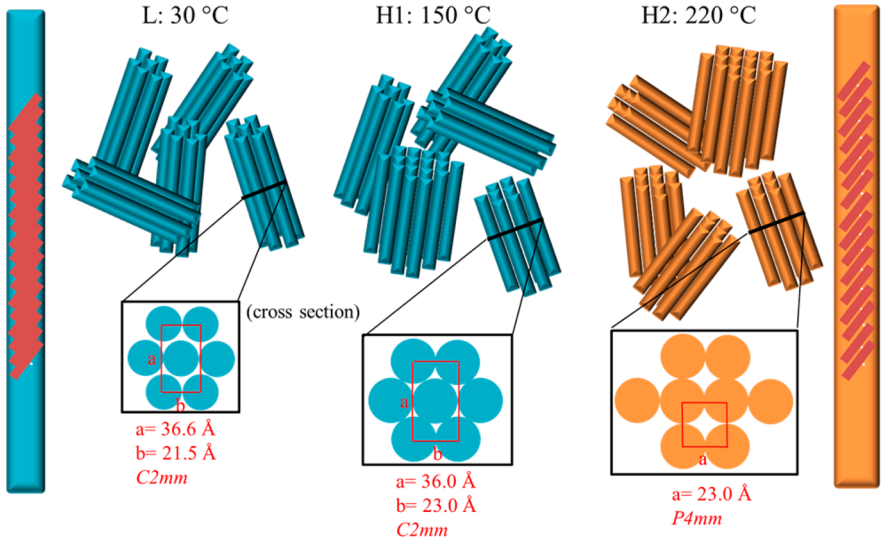


**Figure 12.** Plausible explanation of the reversible phase transition behavior of di(HTh2BT)DTCTT in the L, H1, and H2 phase. The blue and orange columns represent the slip-stacked form of the molecular self-assembly.

$b$ = 23.0 Å at 150 °C. The diameter of the column is estimated to be around 21.5−23.0 Å, which is in good agreement with the slip-stacked geometry. The H1/H2 transition is a more dramatic transition, and the H2 phase is assigned as the 2D rectangular shape (*P4mm*) with $a$ = 23.0 Å at 220 °C. In this case, clusters of columns realign to accommodate the molecular reorganization during the phase transition. Such a drastic motion is assumed to induce mechanical stress and strain, and the cracks observed in the POM image can be attributed to this movement. It is worth noting that the diameter of the column does not change (23 Å), but the peaks in the wide-angle regime shift to lower angles. This indicates that the slip-stacked mode of $\pi-\pi$ stacking is reorganized in a different manner but still maintains a 1D organization. As a whole, the columnar liquid crystal-like phase transitions can explain the reorganization of the packing structure, and it matches well with the other experimental results; however, several low-intensity peaks remain unassigned. The three-dimensional packing structure and structural defects such as rotational isomers could be the reason for the observed deviation. The XRD patterns of di(C12Th2BT)DTCTT can be also assigned as the similar columnar phases (Figure S12). This unique solid-state character of DTCTT derivatives arises from the molecular structure which provides the combination of attractive forces through the core−core interaction, repulsive forces from bulky phenyl side groups, and rotational freedom of the thiophene end groups.

## CONCLUSIONS

We have synthesized fused-ladder thienoarenes, the DTCTT and IDT, substituted with benzothiadiazole and alkyl thiophene side groups. DSC measurement revealed the rich solid-state phases of the system depending on the central core and end group structures. The crystal structure of di(HTh1BT)IDT solved by single crystal XRD explained why the IDT-based molecules remain amorphous; the bulkiness of the hexylphenyl side groups relative to the smaller size of the central core results in a distorted intramolecular conformation without strong backbone interactions, resulting in a lack of periodic $\pi-\pi$ stacking. The S−S interactions seem to play an important role in stabilizing the structure of this molecular system. On the other hand, the crystallinity of the DTCTT derivatives was


DOI: 10.1021/acs.chemmater.7b01226
*Chem. Mater.* 2017, 29, 7686−7696

increased due to the incorporation of the thienothiophene unit. In the presence of the flexible side groups (R = $R_2$ and $R_3$), an unusual thermally induced reversible phase transition behavior was observed. The crystal-to-crystal phase transitions with continuous (L/H1) and discontinuous (H1/H2) phase transition were investigated in detail. Both experimental and computational results revealed that the DTCTT derivatives form a structure with a slip-stacked mode of $\pi-\pi$ stacking and columnar 1D organization, and the structure of each phase was assigned with their 2D lattice symmetries. A combination of both the strong core−core interactions in the slip-stacked form and the flexibility of side groups was assumed to be the key factor for enhancing the molecular reorganization. The 1D organization and $\pi-\pi$ stacking manner is favorable to electronic applications. In fact, this assumption is evidenced by preliminary hole mobility measurement in the OFET device (Figure S13), resulting in the value of $1.9 \times 10^{-2}$ $cm^2/(V \cdot s)$ for the di(HTh2BT)DTCTT film which is 2 orders of magnitude higher than $3.0 \times 10^{-4}$ $cm^2/(V \cdot s)$ of the amorphous di(HTh2BT)IDT film. Manipulating molecular reorganization using weak intermolecular interactions such as S−S interactions has been attempted to develop novel functionality in molecular crystals.[56] This research provides evidence of advanced crystal engineering which opens up an interesting possibility such as controlling semiconducting properties through reorganization of molecular alignment induced by post-thermal treatment.

## ■ ASSOCIATED CONTENT

### Supporting Information

The Supporting Information is available free of charge on the ACS Publications website at DOI: 10.1021/acs.chemmater.7b01226.

Crystallographic information file (CIF)

Details of synthesis and characterization of the DTCTT- and IDT-based molecules, UV−vis, DSC, POM, PXRD, SWAXS, thermal expansion analysis, AFM, DFT calculation, structural assignment of di(C12Th2BT)-DTCTT, and summary of X-ray crystallography of di(HTh1BT)IDT (PDF)

## ■ AUTHOR INFORMATION


### Corresponding Author

*(Y.M.L.) E-mail: ymlam@ntu.edu.sg.

### ORCID

Yuichiro Abe: 0000-0003-4283-8509

Andrew C. Grimsdale: 0000-0003-2498-3024

Michael F. Toney: 0000-0002-7513-1166

Yeng Ming Lam: 0000-0001-9390-8074


### Notes

The authors declare no competing financial interest.

CCDC 1504077 contains the supplementary crystallographic data for this paper. This data can be obtained free of charge from The Cambridge Crystallographic Data Centre via www.ccdc.cam.ac.uk/data_request/cif.

## ■ ACKNOWLEDGMENTS

GI-WAXS measurement was undertaken on the use of the Stanford Synchrotron Radiation Lightsource, SLAC National Accelerator Laboratory, supported by the U.S. Department of Energy, Office of Science, Office of Basic Energy Sciences, under Contract No. DE-AC02-76SF00515. We would like to acknowledge the Facility for Analysis, Characterization, Testing and Simulation, Nanyang Technological University, Singapore, for use of their X-ray facilities. Additionally, we gratefully acknowledge Dr. Sandra Desvergne-Bléneau (Xenocs, Sassenage, France) who performed temperature-variable SWAXS. We also gratefully acknowledge Dr. Bruno Donnadieu (Department of Chemistry, Faculty of Science at National University of Singapore) for his assistance of single-crystal XRD and Dr. Francesco Maddalena (School of Physical and Mathematical Sciences, Nanyang Technological University) for his thoughtful discussion and suggestions. Victoria Savikhin is supported by the Department of Defense (DoD) through the National Defense Science & Engineering Graduate Fellowship (NDSEG) Program.

## ■ REFERENCES


(1) Henson, Z. B.; Mullen, K.; Bazan, G. C. Design strategies for organic semiconductors beyond the molecular formula. *Nat. Chem.* **2012**, *4*, 699−704.

(2) Chen, Y.; Wan, X.; Long, G. High Performance Photovoltaic Applications Using Solution-Processed Small Molecules. *Acc. Chem. Res.* **2013**, *46*, 2645−2655.

(3) Liu, Y.; Chen, C. C.; Hong, Z.; Gao, J.; Yang, Y. M.; Zhou, H.; Dou, L.; Li, G.; Yang, Y. Solution-processed small-molecule solar cells: breaking the 10% power conversion efficiency. *Sci. Rep.* **2013**, *3*, 3356.

(4) van der Poll, T. S.; Love, J. A.; Nguyen, T. Q.; Bazan, G. C. Non-basic high-performance molecules for solution-processed organic solar cells. *Adv. Mater.* **2012**, *24*, 3646−3649.

(5) Kan, B.; Zhang, Q.; Li, M.; Wan, X.; Ni, W.; Long, G.; Wang, Y.; Yang, X.; Feng, H.; Chen, Y. Solution-processed organic solar cells based on dialkylthiol-substituted benzodithiophene unit with efficiency near 10%. *J. Am. Chem. Soc.* **2014**, *136*, 15529−15532.

(6) Coughlin, J. E.; Zhugayevych, A.; Bakus, R. C.; van der Poll, T. S.; Welch, G. C.; Teat, S. J.; Bazan, G. C.; Tretiak, S. A Combined Experimental and Theoretical Study of Conformational Preferences of Molecular Semiconductors. *J. Phys. Chem. C* **2014**, *118*, 15610−15623.

(7) van der Poll, T. S.; Zhugayevych, A.; Chertkov, E.; Bakus, R. C., 2nd; Coughlin, J. E.; Teat, S. J.; Bazan, G. C.; Tretiak, S. Polymorphism of Crystalline Molecular Donors for Solution-Processed Organic Photovoltaics. *J. Phys. Chem. Lett.* **2014**, *5*, 2700−2704.

(8) Zhugayevych, A.; Postupna, O.; Bakus, R. C., II; Welch, G. C.; Bazan, G. C.; Tretiak, S. Ab Initio Study of a Molecular Crystal for Photovoltaics: Light Absorption, Exciton and Charge Carrier Transport. *J. Phys. Chem. C* **2013**, *117*, 4920−4930.

(9) Love, J. A.; Proctor, C. M.; Liu, J.; Takacs, C. J.; Sharenko, A.; van der Poll, T. S.; Heeger, A. J.; Bazan, G. C.; Nguyen, T.-Q. Film Morphology of High Efficiency Solution-Processed Small-Molecule Solar Cells. *Adv. Funct. Mater.* **2013**, *23*, 5019−5026.

(10) Proctor, C. M.; Love, J. A.; Nguyen, T.-Q. Mobility Guidelines for High Fill Factor Solution-Processed Small Molecule Solar Cells. *Adv. Mater.* **2014**, *26*, 5957−5961.

(11) Chung, H.; Diao, Y. Polymorphism as an emerging design strategy for high performance organic electronics. *J. Mater. Chem. C* **2016**, *4*, 3915−3933.

(12) Wombacher, T.; Gassmann, A.; Foro, S.; von Seggern, H.; Schneider, J. J. Structural Polymorphism and Thin Film Transistor Behavior in the Fullerene Framework Molecule 5,6;11,12-di-o-Phenylenetetracene. *Angew. Chem., Int. Ed.* **2016**, *55*, 6041−6046.

(13) Zhang, L.; Colella, N. S.; Cherniawski, B. P.; Mannsfeld, S. C.; Briseno, A. L. Oligothiophene semiconductors: synthesis, characterization, and applications for organic devices. *ACS Appl. Mater. Interfaces* **2014**, *6*, 5327−5343.

(14) Purdum, G. E.; Yao, N.; Woll, A.; Gessner, T.; Weitz, R. T.; Loo, Y.-L. Understanding Polymorph Transformations in Core-Chlorinated Naphthalene Diimides and their Impact on Thin-Film Transistor Performance. *Adv. Funct. Mater.* **2016**, *26*, 2357−2364.

(15) Diao, Y.; Lenn, K. M.; Lee, W. Y.; Blood-Forsythe, M. A.; Xu, J.; Mao, Y.; Kim, Y.; Reinspach, J. A.; Park, S.; Aspuru-Guzik, A.; Xue, G.; Clancy, P.; Bao, Z.; Mannsfeld, S. C. Understanding polymorphism in organic semiconductor thin films through nanoconfinement. *J. Am. Chem. Soc.* **2014**, *136*, 17046−17057.
(16) Jones, A. O. F.; Chattopadhyay, B.; Geerts, Y. H.; Resel, R. Substrate-Induced and Thin-Film Phases: Polymorphism of Organic Materials on Surfaces. *Adv. Funct. Mater.* **2016**, *26*, 2233−2255.
(17) Chen, J.; Shao, M.; Xiao, K.; Rondinone, A. J.; Loo, Y.-L.; Kent, P. R. C.; Sumpter, B. G.; Li, D.; Keum, J. K.; Diemer, P. J.; Anthony, J. E.; Jurchescu, O. D.; Huang, J. Solvent-type-dependent polymorphism and charge transport in a long fused-ring organic semiconductor. *Nanoscale* **2014**, *6*, 449−456.
(18) Chen, J.; Shao, M.; Xiao, K.; He, Z.; Li, D.; Lokitz, B. S.; Hensley, D. K.; Kilbey, S. M.; Anthony, J. E.; Keum, J. K.; Rondinone, A. J.; Lee, W.-Y.; Hong, S.; Bao, Z. Conjugated Polymer-Mediated Polymorphism of a High Performance, Small-Molecule Organic Semiconductor with Tuned Intermolecular Interactions, Enhanced Long-Range Order, and Charge Transport. *Chem. Mater.* **2013**, *25*, 4378−4386.
(19) Iino, H.; Usui, T.; Hanna, J. Liquid crystals for organic thin-film transistors. *Nat. Commun.* **2015**, *6*, 6828.
(20) Laschat, S.; Baro, A.; Steinke, N.; Giesselmann, F.; Hagele, C.; Scalia, G.; Judele, R.; Kapatsina, E.; Sauer, S.; Schreivogel, A.; Tosoni, M. Discotic liquid crystals: from tailor-made synthesis to plastic electronics. *Angew. Chem., Int. Ed.* **2007**, *46*, 4832−4887.
(21) Funahashi, M. Development of Liquid-Crystalline Semiconductors with High Carrier Mobilities and Their Application to Thin-film Transistors. *Polym. J.* **2009**, *41*, 459−469.
(22) Takeda, T.; Tsutsumi, J. y.; Hasegawa, T.; Noro, S.-i.; Nakamura, T.; Akutagawa, T. Electron-deficient acene-based liquid crystals: dialkoxydicyanopyrazinoquinoxalines. *J. Mater. Chem. C* **2015**, *3*, 3016−3022.
(23) Liu, X.; Usui, T.; Hanna, J. A Windmill-Shaped Discotic Columnar Liquid Crystal with Fast Ambipolar Charge Carrier Transport. *Chem. Mater.* **2014**, *26*, 5437−5440.
(24) Abe, Y.; Li, H.; Yin, J.; Soci, C.; Grimsdale, A. C.; Lam, Y. M. A fused thieno[3,2-b]thiophene-dithiophene based donor molecule for organic photovoltaics: a structural comparative study with indaceno-dithiophene. *J. Mater. Chem. C* **2016**, *4*, 9656−9663.
(25) Herbstein, F. On the mechanism of some first-order enantiotropic solid-state phase transitions: from Simon through Ubbelohde to Mnyukh. *Acta Crystallogr., Sect. B: Struct. Sci.* **2006**, *62*, 341−383.
(26) Threlfall, T. L. Analysis of organic polymorphs. A review. *Analyst* **1995**, *120*, 2435−2460.
(27) Jurchescu, O. D.; Mourey, D. A.; Subramanian, S.; Parkin, S. R.; Vogel, B. M.; Anthony, J. E.; Jackson, T. N.; Gundlach, D. J. Effects of polymorphism on charge transport in organic semiconductors. *Phys. Rev. B: Condens. Matter Mater. Phys.* **2009**, *80*, 085201.
(28) Mutai, T.; Satou, H.; Araki, K. Reproducible on-off switching of solid-state luminescence by controlling molecular packing through heat-mode interconversion. *Nat. Mater.* **2005**, *4*, 685−687.
(29) Zhang, B.; Wang, J.; Yu, Z.-Q.; Yang, S.; Shi, A.-C.; Chen, E.-Q. Novel optical anisotropy of a liquid crystalline "cubic" phase in a discotic crown ether derivative. *J. Mater. Chem. C* **2014**, *2*, 5168−5175.
(30) Horie, M.; Suzaki, Y.; Hashizume, D.; Abe, T.; Wu, T.; Sassa, T.; Hosokai, T.; Osakada, K. Thermally-induced phase transition of pseudorotaxane crystals: changes in conformation and interaction of the molecules and optical properties of the crystals. *J. Am. Chem. Soc.* **2012**, *134*, 17932−17944.
(31) Peng, H.; Ran, C.; Liu, Z.; Long, Y.; Wang, Z.; Yu, Z.; Sun, H.; Wei, Y.; Gao, S.; Chen, Z.; Chen, E.-Q. Structure, Physical Properties and Phase Transition of a Quasi-One-Dimensional Organic Semiconductor DBA(TCNQ)2. *J. Phys. Chem. C* **2008**, *112*, 11001−11006.
(32) Tang, Y. Z.; Yu, Y. M.; Xiong, J. B.; Tan, Y. H.; Wen, H. R. Unusual High-Temperature Reversible Phase-Transition Behavior, Structures, and Dielectric-Ferroelectric Properties of Two New Crown Ether Clathrates. *J. Am. Chem. Soc.* **2015**, *137*, 13345−13351.
(33) Harada, J.; Shimojo, T.; Oyamaguchi, H.; Hasegawa, H.; Takahashi, Y.; Satomi, K.; Suzuki, Y.; Kawamata, J.; Inabe, T. Directionally tunable and mechanically deformable ferroelectric crystals from rotating polar globular ionic molecules. *Nat. Chem.* **2016**, *8*, 946−952.
(34) Alarco, P.-J.; Abu-Lebdeh, Y.; Abouimrane, A.; Armand, M. The plastic-crystalline phase of succinonitrile as a universal matrix for solid-state ionic conductors. *Nat. Mater.* **2004**, *3*, 476−481.
(35) Luo, J.; Jensen, A. H.; Brooks, N. R.; Sniekers, J.; Knipper, M.; Aili, D.; Li, Q.; Vanroy, B.; Wubbenhorst, M.; Yan, F.; Van Meervelt, L.; Shao, Z.; Fang, J.; Luo, Z.-H.; De Vos, D. E.; Binnemans, K.; Fransaer, J. 1,2,4-Triazolium perfluorobutanesulfonate as an archetypal pure protic organic ionic plastic crystal electrolyte for all-solid-state fuel cells. *Energy Environ. Sci.* **2015**, *8*, 1276−1291.
(36) Liu, G.; Liu, J.; Ye, X.; Nie, L.; Gu, P.; Tao, X.; Zhang, Q. Self-Healing Behavior in a Thermo-Mechanically Responsive Cocrystal during a Reversible Phase Transition. *Angew. Chem., Int. Ed.* **2017**, *56*, 198−202.
(37) Debenedetti, P. G.; Stillinger, F. H. Supercooled liquids and the glass transition. *Nature* **2001**, *410*, 259−267.
(38) Khamar, D.; Zeglinski, J.; Mealey, D.; Rasmuson, Å. C. Investigating the Role of Solvent−Solute Interaction in Crystal Nucleation of Salicylic Acid from Organic Solvents. *J. Am. Chem. Soc.* **2014**, *136*, 11664−11673.
(39) Korevaar, P. A.; Schaefer, C.; de Greef, T. F.; Meijer, E. W. Controlling chemical self-assembly by solvent-dependent dynamics. *J. Am. Chem. Soc.* **2012**, *134*, 13482−13491.
(40) Sullivan, R. A.; Davey, R. J.; Sadiq, G.; Dent, G.; Back, K. R.; ter Horst, J. H.; Toroz, D.; Hammond, R. B. Revealing the Roles of Desolvation and Molecular Self-Assembly in Crystal Nucleation from Solution: Benzoic andp-Aminobenzoic Acids. *Cryst. Growth Des.* **2014**, *14*, 2689−2696.
(41) McCulloch, I.; Heeney, M.; Bailey, C.; Genevicius, K.; Macdonald, I.; Shkunov, M.; Sparrowe, D.; Tierney, S.; Wagner, R.; Zhang, W.; Chabinyc, M. L.; Kline, R. J.; McGehee, M. D.; Toney, M. F. Liquid-crystalline semiconducting polymers with high charge-carrier mobility. *Nat. Mater.* **2006**, *5*, 328−333.
(42) Takimiya, K.; Osaka, I.; Mori, T.; Nakano, M. Organic semiconductors based on [1]benzothieno[3,2-b][1]benzothiophene substructure. *Acc. Chem. Res.* **2014**, *47*, 1493−1502.
(43) Park, J. I.; Chung, J. W.; Kim, J. Y.; Lee, J.; Jung, J. Y.; Koo, B.; Lee, B. L.; Lee, S. W.; Jin, Y. W.; Lee, S. Y. Dibenzothiopheno[6,5-b:6′,5′-f]thieno[3,2-b]thiophene (DBTTT): High-Performance Small-Molecule Organic Semiconductor for Field-Effect Transistors. *J. Am. Chem. Soc.* **2015**, *137*, 12175−12178.
(44) Haas, S.; Batlogg, B.; Besnard, C.; Schiltz, M.; Kloc, C.; Siegrist, T. Large uniaxial negative thermal expansion in pentacene due to steric hindrance. *Phys. Rev. B: Condens. Matter Mater. Phys.* **2007**, *76*, 205203−205207.
(45) Das, D.; Jacobs, T.; Pietraszko, A.; Barbour, L. J. Anomalous thermal expansion of an organic crystal-implications for elucidating the mechanism of an enantiotropic phase transformation. *Chem. Commun.* **2011**, *47*, 6009−6011.
(46) Li, Y.; Coropceanu, V.; Brédas, J.-L. Thermal Narrowing of the Electronic Bandwidths in Organic Molecular Semiconductors: Impact of the Crystal Thermal Expansion. *J. Phys. Chem. Lett.* **2012**, *3*, 3325−3329.
(47) Gann, E.; Gao, X. K.; Di, C. A.; McNeill, C. R. Phase Transitions and Anisotropic Thermal Expansion in High Mobility Core-expanded Naphthalene Diimide Thin Film Transistors. *Adv. Funct. Mater.* **2014**, *24*, 7211−7220.
(48) Das, D.; Jacobs, T.; Barbour, L. J. Exceptionally large positive and negative anisotropic thermal expansion of an organic crystalline material. *Nat. Mater.* **2010**, *9*, 36−39.
(49) Hoeben, F. J. M.; Jonkheijm, P.; Meijer, E. W.; Schenning, A. P. H. J. About Supramolecular Assemblies of π-Conjugated Systems. *Chem. Rev.* **2005**, *105*, 1491−1546.


DOI: 10.1021/acs.chemmater.7b01226
*Chem. Mater.* 2017, 29, 7686−7696

(50) Yadav, A.; Mishra, P. C. Dimers and trimers of polycyclic aromatic hydrocarbons as models of graphene bilayers and trilayers: enhanced electron density at the edges. *Mol. Phys.* **2014**, *112*, 88−96.
(51) Shearman, G. C.; Yahioglu, G.; Kirstein, J.; Milgrom, L. R.; Seddon, J. M. Synthesis and phase behaviour of *β*-octaalkyl porphyrins. *J. Mater. Chem.* **2009**, *19*, 598−604.
(52) Morale, F.; Date, R. W.; Guillon, D.; Bruce, D. W.; Finn, R. L.; Wilson, C.; Blake, A. J.; Schroder, M.; Donnio, B. Columnar mesomorphism from hemi-disklike metallomesogens derived from 2,6-bis[3′,4′,5′-tri(alkoxy)phenyliminomethyl]pyridines (L): crystal and molecular structures of [M(L)Cl2] (M = Mn, Ni, Zn). *Chem. - Eur. J.* **2003**, *9*, 2484−2501.
(53) Kaller, M.; Tussetschlager, S.; Fischer, P.; Deck, C.; Baro, A.; Giesselmann, F.; Laschat, S. Columnar mesophases controlled by counterions in potassium complexes of dibenzo[18]crown-6 derivatives. *Chem. - Eur. J.* **2009**, *15*, 9530−9542.
(54) Wohrle, T.; Wurzbach, I.; Kirres, J.; Kostidou, A.; Kapernaum, N.; Litterscheidt, J.; Haenle, J. C.; Staffeld, P.; Baro, A.; Giesselmann, F.; Laschat, S. Discotic Liquid Crystals. *Chem. Rev.* **2016**, *116*, 1139−1241.
(55) There are some small peaks which are not assigned with the indicated symmetricity. They comes from either symmetry violation (i.e., 2theta = 4.1 and 7.3 for L phase, 3.9 and 6.4 for H1 phase) or possible contaminated phases.
(56) Commins, P.; Hara, H.; Naumov, P. Self-Healing Molecular Crystals. *Angew. Chem., Int. Ed.* **2016**, *55*, 13028−13032.



DOI: 10.1021/acs.chemmater.7b01226
*Chem. Mater.* 2017, 29, 7686−7696